UC San Diego
UC San Diego Previously Published Works

Title

Improved quantification and mapping of anomalous pulmonary venous flow with four-dimensional phase-contrast MRI and interactive streamline rendering

Permalink

Journal

ISSN

Authors

Hsiao, Albert
Yousaf, Ufra
Alley, Marcus T
et al.

Publication Date

DOI

Peer reviewed

Improved Quantification and Mapping of Anomalous Pulmonary Venous Flow With Four-Dimensional Phase-Contrast MRI and Interactive Streamline Rendering

Albert Hsiao, MD, PhD,[1]* Ufra Yousaf, MBBS,[2] Marcus T. Alley, PhD,[2]
Michael Lustig, PhD,[3] Frandics Pak Chan, MD, PhD,[2] Beverley Newman, MD,[2]
and Shreyas S. Vasanawala, MD, PhD[2]

Background: Cardiac MRI is routinely performed for quantification of shunt flow in patients with anomalous pulmonary veins, but can be technically-challenging to perform. Four-dimensional phase-contrast (4D-PC) MRI has potential to simplify this exam. We sought to determine whether 4D-PC may be a viable clinical alternative to conventional 2D phase-contrast MR imaging.

Methods: With institutional review board approval and HIPAA-compliance, we retrospectively identified all patients with anomalous pulmonary veins who underwent cardiac MRI at either 1.5 Tesla (T) or 3T with parallel-imaging compressed-sensing (PI-CS) 4D-PC between April, 2011 and October, 2013. A total of 15 exams were included (10 male, 5 female). Algorithms for interactive streamline visualization were developed and integrated into in-house software. Blood flow was measured at the valves, pulmonary arteries and veins, cavae, and any associated shunts. Pulmonary veins were mapped to their receiving atrial chamber with streamlines. The intraobserver, interobserver, internal consistency of flow measurements, and consistency with conventional MRI were then evaluated with Pearson correlation and Bland-Altman analysis.

Results: Triplicate measurements of blood flow from 4D-PC were highly consistent, particularly at the aortic and pulmonary valves (cv 2–3%). Flow measurements were reproducible by a second observer ($\rho = 0.986$–0.999). Direct measurements of shunt volume from anomalous veins and intracardiac shunts matched indirect estimates from the outflow valves ($\rho = 0.966$). Measurements of shunt fraction using 4D-PC using any approach were more consistent with ventricular volumetric displacements than conventional 2D-PC ($\rho = 0.972$–0.991 versus 0.929).

Conclusion: Shunt flow may be reliably quantified with 4D-PC MRI, either indirectly or with detailed delineation of flow from multiple shunts. The 4D-PC may be a more accurate alternative to conventional MRI.

J. MAGN. RESON. IMAGING 2015;00:000–000.

Diagnostic evaluation of patients with anomalous pulmonary venous return is essential for assessment before and after surgical repair. Though invasive catheter-based angiography was historically the mainstay of diagnosis, non-invasive imaging techniques, including computed tomography (CT), MRI, and echocardiography (ECHO) are increasingly used for characterizing the nature of anomalous venous drainage pathways and assessment of potential surgi-cal complications.[1–5] Each of these modalities has characteristic limitations, including limited sonographic windows for ECHO and radiation exposure for CT. Although it is possible with MRI to routinely visualize anomalous pulmonary venous drainage, identify any associated shunts, and quantify the severity of intracardiac and extracardiac shunting,[4] comprehensive delineation of multiple contributions of shunt flow can be costly and time-intensive with

conventional MRI acquisitions. Because of the intrinsically complex anatomy of patients with anomalous pulmonary venous drainage and frequent association with additional shunts, these exams also often require direct physician supervision, further contributing to the overall cost of conventional MRI.

4D phase-contrast MRI (4D-PC), is an evolving imaging technique that has recently benefited from rapid developments in parallel-imaging and compressed-sensing.[6–9] These improvements have markedly reduced acquisition times, enabling clinical use. Several studies have now shown the qualitative and quantitative utility of this approach for routine evaluation of structural heart disease.[10] The 4D-PC appears to preserve, and in certain circumstances, even improve upon the quantitative reliability of conventional phase-contrast MRI for quantifying cardiac blood flow and valve function.[11] Furthermore, flow measurements from 4D-PC have been shown to better correlate with ventricular volumetric displacement than conventional phase-contrast MRI.[12] The qualitative diagnostic utility of 4D-PC has been shown to be comparable to ECHO for identification of valvular insufficiency and intracardiac shunts, while improving visualization of extracardiac shunts.[13] Previous work also showed that using the parallel-imaging and compressed-sensing variant of 4D-PC, venous flow measurements may be obtained with comparable precision and accuracy to arterial flow measurements at high velocity-encoding speeds.[14]

These early experiences with 4D-PC have raised the possibility that this imaging technique may by itself be sufficient for comprehensive diagnostic evaluation of structural heart disease in certain patient populations. In particular, we hypothesize that 4D-PC may simplify evaluation of patients with pulmonary venous anomalies, before and after repair. The complex and variable nature of pulmonary venous drainage in these patients is otherwise very time-intensive to fully evaluate by conventional planar MRI.[15] At the present time, however, software tools for interpreting and interrogating 4D-PC data have limited functionality for detailed analysis of flow connectivity. In particular, it can be difficult on anatomic imaging alone to visually track pulmonary veins to their target atria and distinguish them from adjacent vessels, whether by CT or MRI. Furthermore, the reliability of 4D-PC for quantifying pulmonary venous shunting has not been studied. We therefore sought to develop strategies for using our previously reported and validated variant of 4D-PC to quantify flow from anomalous pulmonary veins. Specifically, we devised an interactive streamline rendering approach to map pulmonary veins to their receiving chambers, used these to directly quantify pulmonary shunt flow, and compared the consistency of these flow measurements with indirect shunt fractions obtained with 4D-PC, conventional 2D-PC, and SSFP volumetry.

Materials and Methods

Subjects

With institutional review board approval and HIPAA compliance, we retrospectively identified all patients with partial or total anomalous pulmonary venous return for whom an accelerated, parallel-imaging and compressed-sensing 4D-PC acquisition [12,13] of the whole chest was performed as part of a routine clinical MRI examination from April of 2011 through October of 2013. This included 11 patients with anomalous venous drainage and 4 patients following repair without residual shunts. Informed consent for off-label MRI acquisitions was obtained before each exam. A total of 16 examinations were identified. One patient who underwent a 1.5-ventricle repair for double-outlet right ventricle with a Glenn shunt and a Rastelli was excluded from the study, to simplify interpretation of the data. A similar number of patients were scanned at 3 Tesla (T) and 1.5T, though we triaged younger patients requiring general anesthesia to our smaller bore 3T magnet (Table 1).

MRI Technique

MR imaging was performed on a 1.5T TwinSpeed MRI scanner with an eight-channel phased array cardiac coil (GE Healthcare, Milwaukee, WI) for patients before June of 2012. Following this date, MR imaging was either performed on a 3T 750 MRI scanner with a 32-channel phased array cardiac coil (GE Healthcare, Milwaukee, WI) or a 1.5T 450 W MRI scanner with a 32-channel phased array cardiac coil (GE Healthcare, Milwaukee, WI). Vector ECG gating was used. Examinations were performed under cardiac general anesthesia for patients less than 6 years of age (n = 10).

Regardless of magnet and field strength, each 4D-PC acquisition was performed following contrast-enhanced MRA performed with off-label intravenous administration of single-dose gadofosveset. The contrast-enhanced MRA was obtained for clinical reasons, but not used for this study. The 4D-PC MRI was performed using a SPGR-based sequence with simple four-point flow-encoding [16] and variable-density Poisson-disc k-space undersampling [17,18] with total acceleration factors ranging from 2×2 to 2×4 (phase $\times$ slice). Zero-filling interpolation (ZIP) of 2 was applied in the slice direction. Images were reconstructed for each cardiac temporal phase separately with a combined autocalibrating parallel imaging compressed sensing algorithm (L_1-SPIRiT).[19] Compressed-sensing was implemented to take advantage of per-slice 2D spatial sparsity without enforcing temporal sparsity. k-Space phase-reordering was used for respiratory compensation (EXORCIST, GE Healthcare, Milwaukee, WI). No respiratory gating or signal averaging (NEX) was used. Image acquisition parameters are summarized in Table 1. Reported spatial and temporal resolution reflect sampling frequency rather than pixel spacing of the reconstructed images. Data were acquired with segmented k-space, using two to three views/segment, except in one patient with heart rate of 65, where four views/segment was used. The 20 cardiac phases were reconstructed spanning the entire cardiac cycle. Image reconstructions were performed with a GPGPU implementation of L_1-SPIRIT [20] on a 64-bit Linux workstation equipped with four Tesla C1060 graphics cards (NVIDIA, Santa Clara, CA), typically requiring 60 min of total image reconstruction time. Image data were corrected for

TABLE 1. Summary of Demographics and Imaging Parameters for Patients Included in the Study[a]

	1.5T	3.0T	*P*-value
Demographics			
Number of patients	7	8	n/a
Age (years)	11.1 (1.5–21)	2 (0.2–5)	**0.01**
Weight (kg)	35 (10–69)	11 (5–20)	**0.02**
Height (cm)	135 (82–175)	83 (54–113)	**0.01**
BSA (m^2)	8.05 (0.47–50)	0.5 (0.26-0.79)	0.32
Heart rate (bpm)	95 (65–132)	113 (81–141)	0.14
Unrepaired PAPVR	5	6	n/a
Repaired PAPVR	1	0	n/a
Repaired TAPVR	1	2	n/a
General anesthesia	2	8	n/a
4D-PC Parameters			
Flip angle (degrees)	15	15	n/a
Bandwidth (kHz)	62.50	83.33	n/a
Velocity-encoding (cm/s)	181 (120–250)	244 (200–250)	**0.01**
Repetition time (ms)	4.79 (4.31-5.26)	3.44 (3.03–4.43)	**1.9E-05**
Echo time (ms)	1.85 (1.62-2.11)	1.36 (1.23-1.72)	**1.1E-04**
Row resolution (mm)	1.05 (0.86-1.25)	1.07 (0.86-1.35)	0.67
Column resolution (mm)	1.4 (1.15-1.67)	1 (0.86-1.25)	**4.1E-04**
Slice resolution (mm)	2.37 (2–3)	2.31 (2–3)	0.48
Temporal resolution (ms)	57 (34–69)	40 (28–53)	**2.8E-03**
Matrix (row x column)	256 x 192	256 x 192	n/a
Field of view (cm)	27 (22–32)	24 (22–26)	0.07
Slice count (ZIPx2)	129 (100–148)	132 (100–160)	0.44
Views/segment	3 (2–4)	3 (2–3)	0.63
Total acceleration factors (phase x slice)	2 x 2	2 x 3–4	n/a
Scan time (mm:ss)	9:04 (5:28-10:48)	5:17 (3:33-6:52)	**1.9E-03**
Quantitative metrics			
Shunt fraction (Q_p/Q_s)	1.85 (0.94-2.8)	1.85 (1.11-3.68)	**0.98**
Shunt volume (Q_p-Q_s, L/min)	3.23 (−0.29-10.28)	1.35 (0.2–4.31)	**0.27**

[a]In general, younger patients were triaged to be scanned on the 3T and older patients were triaged to the wide-bore 1.5T.

Maxwell phase effects,[21] encoding errors related to gradient field distortions.[22] Eddy-current related phase offsets were corrected using a software-based phase-error model calculated with a second order polynomial fit of stationary voxel data.[12,23]

A summary of image acquisition parameters and patient demographics are shown in Table 1. Younger patients were triaged to the smaller bore 3T MRI. Image acquisition times for 4D-PC averaged 5.28 min at 3T and 8.9 min at 1.5T, with similar spatial and temporal resolution, due to the use of higher acceleration factors at 3T. Representative images from two patients with PAPVR and associated sinus venosus ASD are shown in Figure 1.

Following analysis of 4D-PC data, both flow and ventricular volume data were collated from each MRI exam's corresponding official report, which was based on conventional 2D-PC and planar SSFP imaging. For the conventional portion of the exam, imaging acquisition planes were prescribed and segmentation contours verified by one of three board-certified radiologists with dedicated cardiovascular training and 5 (S.S.V.), 7 (B.N.), and greater than 10 (F.P.C.) years of experience in pediatric cardiovascular MRI. MR technique and postprocessing of conventional 2D-PC and SSFP imaging was performed in the manner previously described.[24]
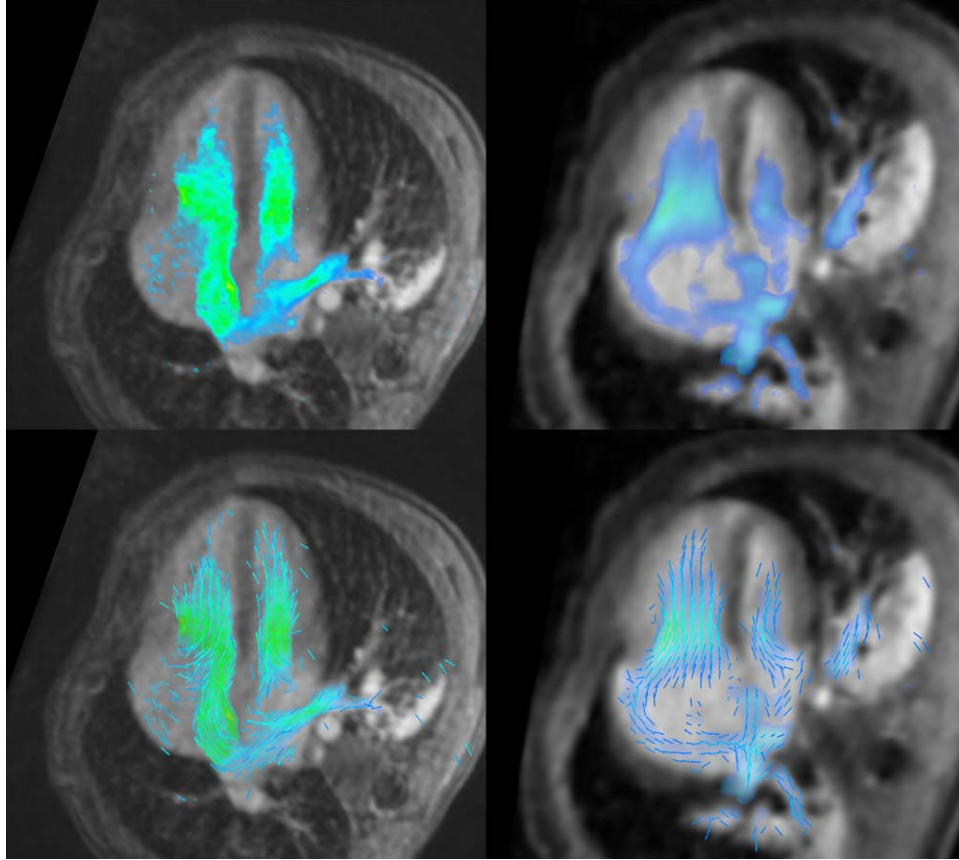
FIGURE 1: Representative images from two infants with unrepaired partial anomalous pulmonary venous return and sinus venosus atrial septal defects. Color velocity and vector-rendered images are shown in the upper and lower panels, respectively. Left: 7-min 1.5T scan of 18-month-old boy (10 kg, 0.5 m^2) with 132 bpm heart rate. Right: 3.5-min 3T scan of a 6-month-old boy (8.33 kg, 0.4 m^2) with 126 bpm heart rate. Note the smoother color-rendering and qualitative consistency of vector field seen at 3T.

Software

Quantitative 4D-PC analysis software, FlowAnalytix, was developed and implemented in Java (version 1.6.0, Oracle) and OpenGL (version 1.1, SGI), building upon a visualization and quantification framework previously described.[11,12,24] For this study, a new interactive method of streamline and pathline visualization was implemented in CUDA (version 5.0, NVIDIA, Santa Clara, CA). Software tools were implemented to allow users to manually define seed points in a 3D interactive manner from the multiplanar reformatted (MPR) display or define seed planes using previously defined vessel segmentations.

Streamlines were computed iteratively from each seed point, iterating by a variable pseudotime, τ_j, for each iteration j, until the total iteration time $\sum_j \tau_j$ exceeded the iteration duration T. Iteration duration T is a user-controlled variable, by default 1000 ms, which specifies the maximum lifetime of any streamline trace. The duration of each iteration pseudotime τ_j was computed based on the local velocity $\vec{v}(\vec{x})$ at the current image position $\vec{x}$ and voxel dimensions $\vec{d}$ with

$$\tau = \min_i(d_i/v_i), \qquad (1)$$

where i indexes each dimension of vectors $\vec{v}$ and $\vec{d}$. The position $\vec{x}$ at each iteration j, was updated with

$$\vec{x}_{j+1} = \vec{x}_j + \tau_j \cdot \vec{v}(\vec{x}_j). \qquad (2)$$

To minimize the need for user-interaction in the streamline rendering, we developed a thresholding system to minimize extraluminal propagation of streamlines without the need for explicit vessel surface segmentation. At each iteration, streamlines were allowed to further propagate if the speed or the signal-speed product both exceeded user-specified rendering thresholds, set by the user with interactive slider controls.

Quantitative Analysis

The quantification of aortic, pulmonary flow and shunting was performed in two stages. Observer 1 (U.Y.) was trained to identify the aortic valve (AV), main pulmonary artery (MPA), right and left pulmonary arteries (RPA, LPA), superior vena cava (SVC), and inferior vena cava (IVC). Blood flow through of these vessels was then measured in triplicate at locations at least 1-mm apart using the in-house developed software, permitting assessment of intra-observer variability. To assess inter-observer variability, a board-certified radiologist (A.H.) with 5 years of experience in congenital cardiac MRI independently performed measurements of the same vessels, henceforth known as observer 2. In addition to the set of measurements obtained by observer 1, observer 2 also quantified flow in each of the pulmonary veins and any other concomitant shunts.

Each of the pulmonary veins was identified from the signal magnitude image data from 4D-PC and manually segmented for

the purposes of flow quantification. Segmentations of the pulmonary veins were further used as seed locations for interactive streamline rendering to map each of the pulmonary veins to their receiving atria. In cases with a concomitant atrial septal defect (ASD), a septal-tracking plane was placed across the flow jet and the ASD was directly quantified. Indirect measurements of shunt fraction (Q_P/Q_S) were computed as the ratio of net flow across the pulmonary valve to the net flow across the aortic valve, where Q_P is the net pulmonary flow and Q_S is the net systemic flow. Indirect measurements of shunt volume (Q_P-Q_S) were similarly obtained. Direct measurements of shunt volume (Q_D) were obtained by summing the volumetric flow rates from each identifiable left-to-right shunt. Direct measurements of shunt fraction were computed according to (Q_{AV}+ Q_D)/Q_{AV}, where Q_{AV} is the flow across the aortic valve.

Statistical Analyses

Statistical analyses were performed with custom macros defined in Excel 2007 (Microsoft, Redmond, WA). From the triplicate measurements obtained by observer 1, we computed coefficients of variation as an estimator of intra-observer variation at each of the measurement locations (AV, MPA, RPA, LPA, SVC, IVC). For the remainder of the study, Pearson correlation and Bland-Altman analysis were used for comparisons of quantitative consistency. Bland-Altman limits of agreement are reported as 1.96 times the standard deviation of errors. To compare interobserver consistency, the mean of triplicate measurements of flow by observer 1 was compared with single measurements from observer 2. Shunt fractions by observer 1 were calculated as the ratio of triplicate measurements of pulmonary and systemic flow. To assess internal consistency, for both observers, flow measurements at the pulmonary valve were compared against the sum of the main and branch pulmonary arteries.

After directly mapping each pulmonary vein to their receiving chambers, it was possible to assess the internal consistency of inflow–outflow flow measurements in multiple ways. Due to the complex geometry of the pulmonary veins, only observer 2 performed these measurements. With these pulmonary venous flow measurements, we were able to compare the consistency of inflow and outflow each lung and of each ventricle, as well as the consistency of shunt fraction and shunt volume measurements obtained directly and indirectly. Finally, with Pearson correlation and Bland-Altman analysis, we further compared measurements by both observers against collated data from clinical reports where 2D-PC flow and SSFP volumes were obtained. The 2D-PC and SSFP data were obtained in 11 of the 15 exams. Locations of 2D-PC measurements were not used to define imaging planes for 4D-PC. None of the patients had more than mild regurgitation at any valve by ECHO or 4D-PC imaging. To identify significant differences in quantitative consistency, we applied *F-tests* with a type I error rate (α) of 0.05.

Results

Intraobserver Repeatability of Flow Measurements

The repeatability of triplicate measurements of blood flow obtained each at the aortic valve, pulmonary valve, right pulmonary artery, left pulmonary artery, SVC and IVC are shown in Table 2. Measurements at the aortic and

TABLE 2. Intraobserver Consistency of Flow Measurements[a]

	AV	PV	RPA	LPA	SVC	IVC
Mean coefficient of variation	3%	2%	4%	4%	4%	6%
Min coefficient of variation	0%	0%	0%	0%	0%	1%
Max coefficient of variation	6%	6%	18%	18%	14%	17%

[a]The mean, minimum, and maximum coefficients of variation are shown along each vessel of interest, taken from triplicate measurements obtained by observer 1. Flow measurements were obtained at the aortic and pulmonary valve were the most consistent between repeated measurements.
AV = aortic valve; PV = pulmonary valve; RPA = right pulmonary artery; LPA = left pulmonary artery; SVC = superior vena cava; IVC = inferior vena cava.

pulmonary valves showed the highest consistency with mean coefficients of variation of 3% and 2%, respectively, and maximum coefficients of variation of 6% each. Measurements of the branch pulmonary arteries, SVC and IVC were also fairly reproducible with mean coefficients of variation of 4–6% and maximum coefficients of variation of 14–18%.

Interobserver Reproducibility of Flow Measurements

The mean of triplicate blood flow measurements were further compared with independent single measurements obtained observer 2, shown in Table 3 and Figure 2. Blood flow measurements were most consistent between observers at the aortic valve, pulmonary valve, right pulmonary artery and left pulmonary artery ($\rho = 0.994$–0.999). For each of these vessels, Bland-Altman mean differences were close to zero (ranging from -1% to 4%) with narrow limits of agreement (-9% to 13% at the aortic valve and -14% to 11% at the pulmonary valve). At the SVC and IVC, the interobserver consistency was slightly more modest ($\rho = 0.986$, 0.987). Bland-Altman mean differences at the cavae were also close to zero (2% at the SVC and 4% at the IVC) with slightly wider limits of agreement (-18% to 22% at the SVC and -24% to 33% at the IVC).

Shunt fractions by each observer were well-matched ($\rho = 0.983$) with narrow Bland-Altman limits of agreement (-20% to 14%). In our population, measured shunt fractions spanned a range of values, from 0.96 to 3.68. Shunt volumes obtained as a difference of the pulmonary and systemic flow showed a similar result. They were also well-matched ($\rho = 0.997$) with narrow Bland-Altman limits of agreement (-0.47 to 0.43 L/min). Observed shunt volumes ranged from -0.22 L/min to 10.28 L/min.

TABLE 3. Interobserver Consistency of Flow Measurements[a]

	AV	PV	RPA	LPA	SVC	IVC	Qp/Qs	Qp-Qs
B-A Mean	2%	−1%	1%	3%	2%	4%	−3%	−0.02
B-A Min	−9%	−13%	−10%	−7%	−17%	−23%	−20%	−0.47
B-A Max	12%	11%	13%	14%	22%	32%	14%	0.43
Pearson (ρ)	0.997	0.999	0.999	0.994	0.986	0.987	0.983	0.997

[a]Bland-Altman limits of agreement and Pearson correlation coefficients are shown to assess consistency between the mean of measurements obtained by observer 1 and single measurements by observer 2. Measurements from the large arterial vessels showed the strongest agreement between observers.
AV = aortic valve; PV = pulmonary valve; RPA = right pulmonary artery; LPA = left pulmonary artery; SVC = superior vena cava; IVC = inferior vena cava; Q_p/Q_s = shunt fraction; Q_p-Q_s = shunt volume.

Pulmonary Venous to Atrial Chamber Flow Mapping

Example images from streamline mapping for two patients are shown in Figure 3. All shunts visualized on 4D-PC image data, including surgical shunts, ASD, VSD, or aorto-pulmonary collateral arteries were directly quantified. Each of the shunts and their contribution to flow are listed in Table 4. Images from several representative cases are shown in Figure 4, including a patient with a straddling sinus venosus defect (see Supplementary Video S1, which is available online).

Internal Consistency of Pulmonary Arterial Flow Measurements

Because both observers obtained measurements of main, right, and left pulmonary arterial flow, we further investigated whether there were any differences in the internal consistency of pulmonary arterial flow measurements, shown in

Table 5. For both observers, pulmonary valve flow matched the sum of branch (right plus left) pulmonary arterial flow ($\rho = 0.995$, 0.996) with narrow Bland-Altman limits of agreement (−18% to 22%, −20% to 17%). There was no statistically significant difference in the internal measurement errors obtained by either observer ($p = 0.21$, F-test).

Internal Consistency of Flow Measurements and Shunt Quantification

With measurements of pulmonary venous flow obtained by observer 2, it was possible to assess the consistency of flow measurements (a) to and from each of the lungs, (b) to and from each of the ventricles, and (c) indirect and direct measurements of shunt fraction and shunt volume. The strength of these relationships is shown in Table 5. Measurements of inflow and outflow at each location were highly consistent ($\rho = 0.975$–0.994), slightly more consistent for the lungs than the ventricles. Measurements of shunt
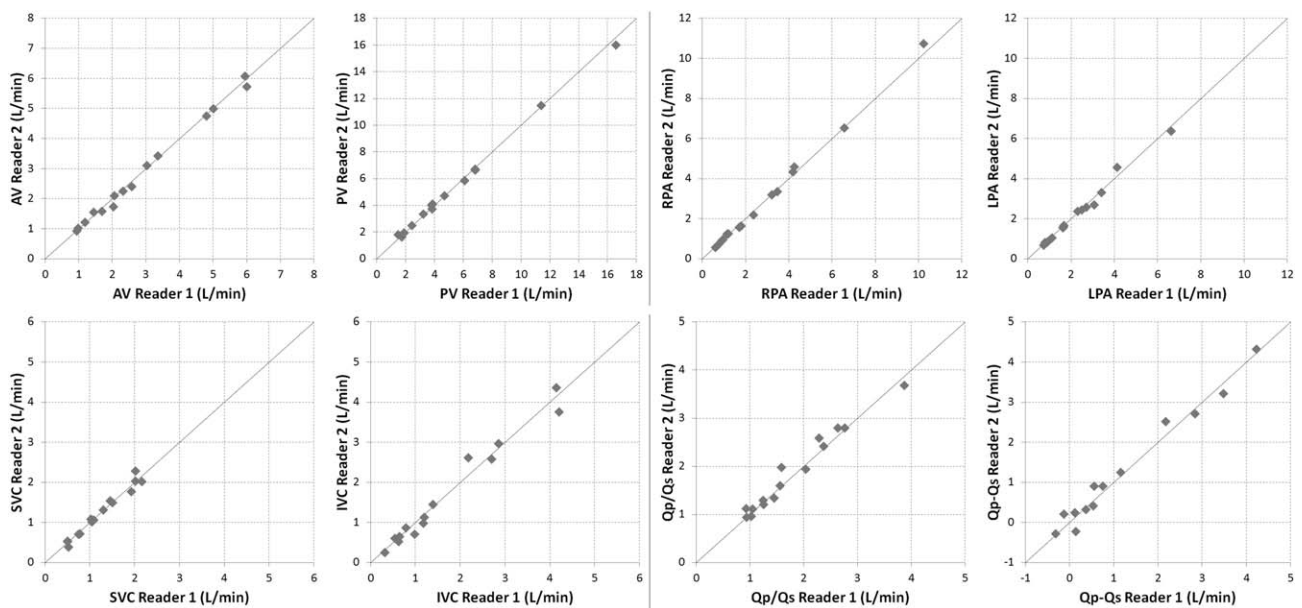

FIGURE 2: Interobserver consistency of flow measurements. Scatter plots display the consistency of flow measurements obtained by each observer at each location and of indirect measurements of shunt fraction and shunt volume. The mean of triplicate measurements by observer 1 (x-axis) were in close agreement with single measurements by observer 2 (y-axis).
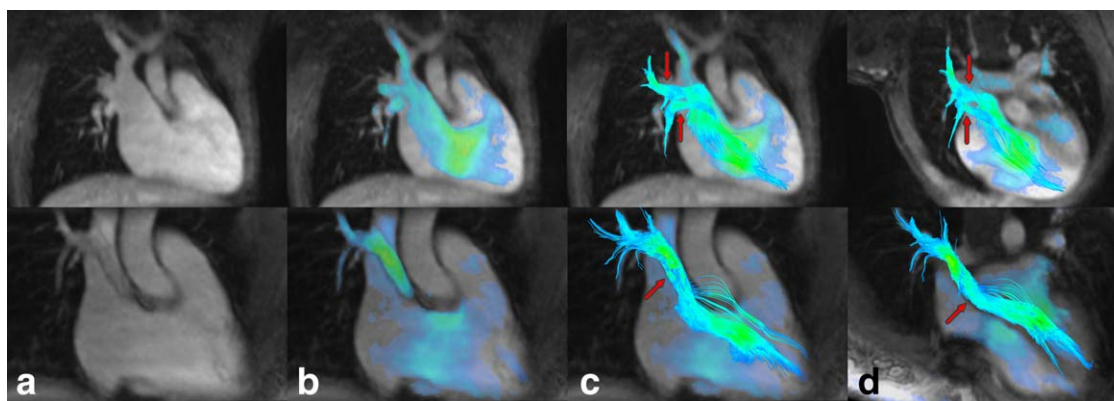
FIGURE 3: Streamline mapping of pulmonary veins to their receiving atrial chambers. Right-ventricular three-chamber and oblique coronal views in mid-diastole with grayscale anatomic rendering (a), color speed overlay (b), and superimposed streamlines (c,d) show the incremental value of each rendering mode for mapping flow from right upper pulmonary veins to the receiving chamber. Top: 3-year-old boy with unrepaired anomalous right upper pulmonary veins, scanned at 3T. Bottom: 21-year-old woman after surgical baffle of the anomalous right upper pulmonary veins to the left atrium, scanned at 1.5T. Note smoother streamlines with the higher signal-to-noise acquisition afforded by the scan performed at 3T.

TABLE 4. Single Flow Measurements (L/min) Obtained With 4D-PC by Observer 2 at the Aortic Valve (AV), Pulmonary Valve (PV), Right and Left Pulmonary Arteries (RPA, LPA), Superior and Inferior Vena Cava (SVC, IVC), Sum of the Pulmonary Veins That Mapped to the Right Atrium (RA), Sum of Pulmonary Veins That Mapped to the Left Atrium (LA), and Any Additional Shunts Identified

| Age	Sex	History	AV	PV	RPA	LPA	SVC	IVC	RA inflow	LA inflow	Other shunts
13 yrs	F	PAPVR, coronary sinus ASD	6.01	16.59	10.23	6.64	2.02	4.21	10.56	7.02	0.00
13 yrs	M	PAPVR, sinus venosus ASD	3.35	6.84	4.19	3.41	0.50	0.65	2.17	5.51	1.60
21 yrs	F	PAPVR, ASD, post-repair	5.95	6.09	3.48	2.49	2.16	4.15	0.00	6.38	0.00
13 yrs	F	TAPVR, post-repair	5.01	4.70	3.22	1.67	1.93	2.71	0.00	5.10	0.00
18 mo	M	PAPVR, sinus venosus ASD	1.69	3.87	2.37	1.65	1.05	0.55	1.21	3.14	1.19
23 mo	M	PAPVR, perimembranous VSD	1.19	1.73	0.61	1.13	0.78	0.63	0.70	1.39	−0.06
14 yrs	M	Total right PAPVR	4.80	11.40	6.56	4.12	2.02	2.86	6.54	4.43	0.00
4 yrs	M	PAPVR	2.06	3.23	1.21	2.31	1.09	0.79	1.80	2.39	0.00
16 mo	F	TAPVR, post-repair with persistent anomalous portal vein to left atrium	1.45	1.83	0.90	0.91	0.75	1.18	0.00	2.12	0.23
6 mo	M	PAPVR, sinus venosus ASD	0.99	3.83	1.80	1.62	0.53	0.98	2.16	1.62	0.63
6 mo	M	PAPVR, straddling sinus venosus ASD	2.03	1.90	0.96	0.73	1.02	0.62	0.59	1.10	−0.58
5 yrs	M	PAPVR with right aortopulmonary collaterals	3.04	3.80	0.77	3.07	1.45	2.18	0.99	3.49	−0.62
3 mo	M	PAPVR, small ASD	0.95	1.50	1.14	0.80	0.50	0.32	0.75	1.08	0.00
3 yrs	M	PAPVR, sinus venosus ASD	2.58	6.82	4.25	2.70	1.30	1.39	1.95	4.09	2.05
18 mo	M	TAPVR, post-repair	2.33	2.45	1.72	0.81	1.50	1.20	0.00	3.17	0.00
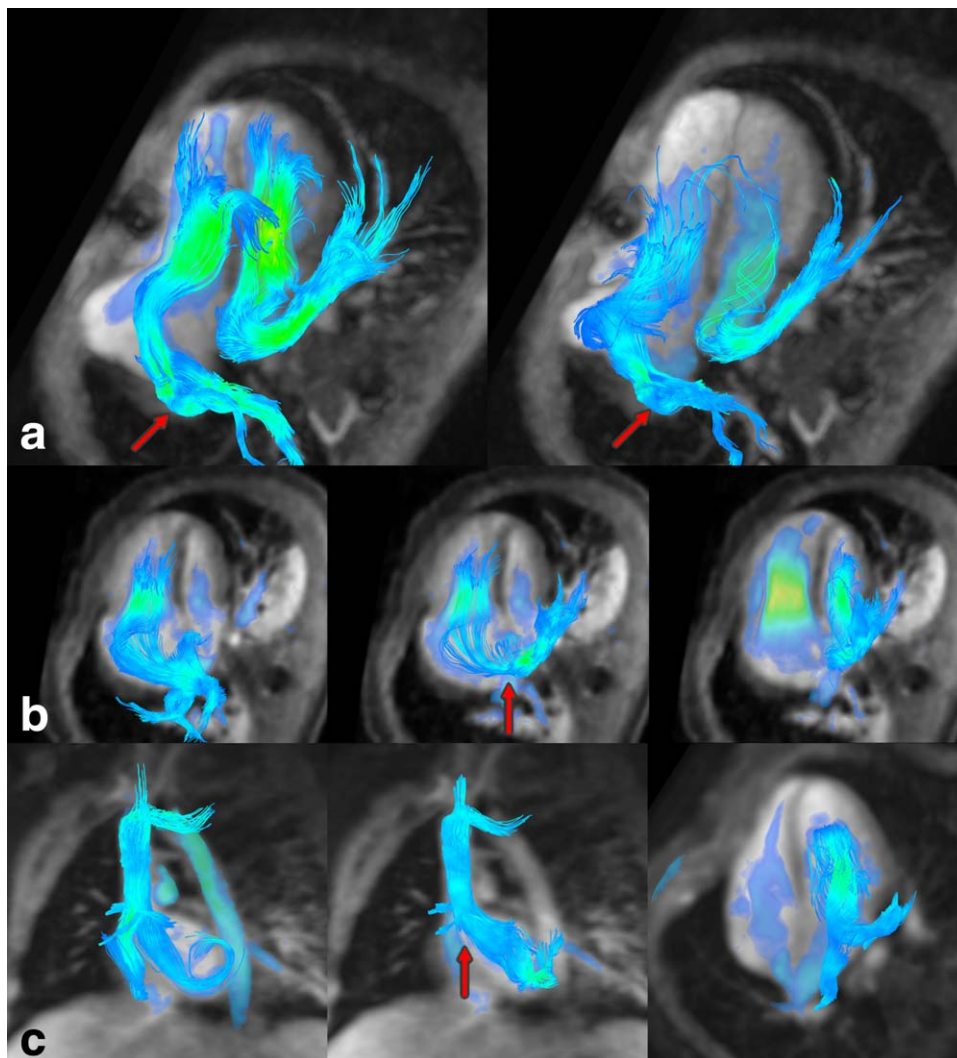
FIGURE 4: Streamline mapping of pulmonary veins to their receiving atrial chambers. a: Four-chamber views during diastole show anomalous right pulmonary veins drain into the right atrium (arrows) and an intact atrial septum. b: Four-chamber views during diastole in another patient also show right pulmonary veins drain to the right atrium. The left pulmonary veins drain normally into the left atrium, though some flow arrives in the right atrium through a sinus venosus ASD (arrow). c: Oblique coronal views from a third patient during systole (left) and diastole (middle) show blood from anomalous pulmonary veins and the SVC draining into both atria through a straddling sinus venosus defect (arrow). Each of the left and one right pulmonary vein drain into the left atrium (right).

fraction and shunt volume were also consistent, whether measured indirectly or directly ($\rho = 0.990$–0.996).

External Comparison With Conventional Phase-Contrast

4D-PC and 2D-PC flow rates were generally consistent, irrespective of which observer performed the 4D-PC measurements ($\rho = 0.962$–0.988; n = 11), shown in Table 6. Shunt fraction and shunt volume measurements by both techniques were also generally consistent ($\rho = 0.897$–0.917; n = 11). However, in some cases, shunt fraction measurements between 2D-PC and 4D-PC varied by as much as 0.85.

External Comparison With Stroke Volume

To further address the occasional discrepancy between 2D-PC and 4D-PC shunt fraction estimation, we further compared with stroke volumes estimated by SSFP volumetry. The 4D-PC measurements showed higher correlation to the SSFP stroke volume ratio than 2D-PC ($\rho = 0.972$–0.991 versus 0.929) with narrower limits of agreement, shown in Figure 5. The difference in the strength of correlation was found to be statistically significant for the ratio of triplicate measurements by observer 1 ($P < 0.05$, *F-test*). The ratio of single measurements by observer 2 also showed narrower limits of agreement, but did not achieve statistical significance in our small patient population ($\rho = 0.396$, *F-test*).

Discussion

We demonstrated here that it is possible to perform a comprehensive, quantitative analysis of sources of shunting in patients with anomalous pulmonary veins with accelerated

TABLE 5. Inflow-Outflow Consistency of Flow Measurements Obtained by Each Observer

	Observer 1	Observer 2						
	PA	PA	Right lung	Left lung	RV	LV	Q_P/Q_S	Q_P-Q_S
B-A Mean	2%	−2%	−7%	−6%	3%	8%	2%	0.05
B-A Min	−17%	−20%	−38%	−29%	−23%	−22%	−13%	−0.46
B-A Max	21%	16%	24%	17%	30%	38%	17%	0.56
Pearson	0.995	0.996	0.994	0.992	0.989	0.975	0.990	0.996
F-test	0.21							

For each location, Bland-Altman limits of agreement and Pearson correlation coefficients are shown, comparing measurements of blood flow into and out of each structure listed. For example, for the PA, flow from the pulmonary valve was compared to the right and left pulmonary arteries. For the right lung, right pulmonary arterial flow was compared to the sum of the pulmonary veins. For the right ventricle, the right atrial inflow and left-to-right ASD and VSD flow was compared to the pulmonary valve. For Q_P/Q_S and Q_P-Q_S, we compared indirect and direct quantification of all identifiable shunts.
PA = main pulmonary artery; RV = right ventricle; LV = left ventricle; Q_P/Q_S = shunt fraction; Q_P-Q_S = shunt volume; ASD = atrial septal defect; VSD = ventricular septal defect.

4D phase-contrast MRI. Although conventional phase-contrast MRI remains the clinical gold standard for noninvasive measurement of blood flow and shunt fraction, it can time-consuming to perform the numerous oblique planes that are required to interrogate the multiple sources of shunting that may be simultaneously present. We have shown here that 4D-PC improves upon this clinical gold standard, spanning a range of shunt fractions. In particular, we showed that flow measurements are highly reproducible by the same or different observers, at different locations along a branching vessel, and at the inflow and outflow of different organs of interest. Most importantly, we found that measurements of shunt fraction (Q_p/Q_s) by 4D-PC are not only reproducible, but show better agreement with the ratio of stroke volumes of the right and left ventricles than conventional 2D-PC based assessment of shunt fraction.

The ratio of pulmonary flow to systemic flow, also known as the shunt fraction, is often used to assess the need for surgical management of congenital shunts. A shunt fraction of 1.5 is generally considered to the benchmark for surgical intervention in patients with PAPVR.[25] It is still routine at some institutions to proceed with invasive catheter-based angiography to assess the severity of shunt lesions to determine the necessity of repair, though MRI has increasingly taken on this role. In our small patient population, although we did identify a few shunt fractions that were rather discrepant between 2D-PC and 4D-PC, none of the shunt fractions crossed this threshold of 1.5, and the thus differences between measured shunt fractions probably would not have changed management.

We describe in this work an approach to postprocessing of 4D-PC data using an approach we have called *interactive streamline rendering*. Currently, the most common approaches for streamline and pathline visualization for 4D-PC data rely on some form of vessel segmentation for streamline visualization.[26] Such segmentations can be time-consuming to perform, especially for smaller vessels. Rather than rely on anatomic segmentation to enable streamline rendering, we propose the reverse in this work—that interactive streamline rendering can instead guide delineation and connectivity of small pulmonary veins. By terminating particle traces at interactive user-specified thresholds, it is possible to use these implicit boundaries without defining explicit ones. This approach may be clinically practical, and

TABLE 6. Consistency of Flow Measurements From 4D-PC and Conventional 2D-PC[a]

	Observer 1				Observer 2			
	AV	PV	Qp/Qs	Qp-Qs	AV	PV	Qp/Qs	Qp-Qs
B-A Mean	−9%	1%	10%	0.65	−6%	−1%	6%	0.63
B-A Min	−24%	−35%	−21%	−2.47	−25%	−38%	−25%	−2.71
B-A Max	6%	37%	41%	3.77	13%	37%	37%	3.98
Pearson	0.988	0.964	0.917	0.901	0.983	0.962	0.901	0.897

[a]Flow measurements were similarly consistent for both observers. The 4D-PC measurements of aortic valve flow were slightly lower than 2D-PC. This had a corresponding impact on shunt fractions and volumes.
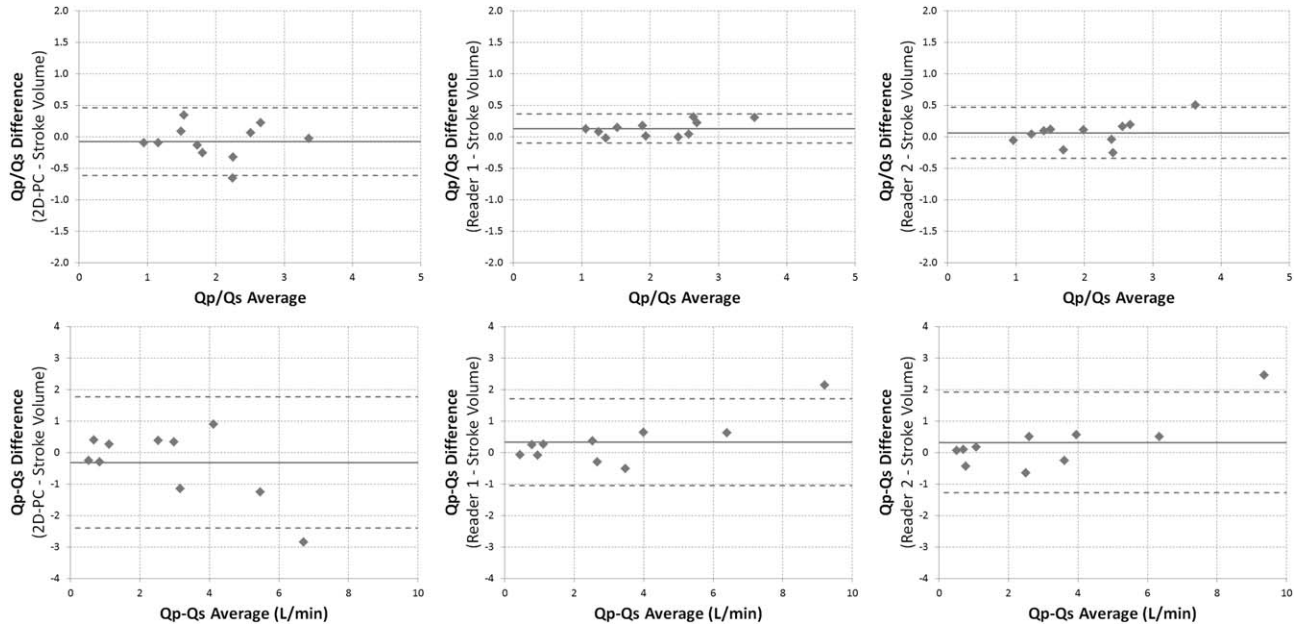
FIGURE 5: Consistency of shunt fraction (top) and shunt volume (bottom) with ventricular volume displacements from SSFP imaging. Bland-Altman plots show that measurements of shunt fraction by conventional phase-contrast and 4D-PC by each observer (middle, right) correlated well with the ratio of right-to-left ventricular stroke volumes. Shunt fractions measured as a ratio of triplicate measurements on 4D-PC by observer 1 were more tightly correlated to ventricular displacements than 2D-PC ($P < 0.05$, F-test). Single measurements on 4D-PC by observer 2 also had narrower limits of agreement to ventricular displacement than 2D-PC, but did not achieve statistical significance.

we found this to be sufficient for mapping the drainage of pulmonary veins.

Interrogation of the pulmonary veins is typically a daunting task for conventional phase-contrast imaging, and thus is rarely performed. The pulmonary venous vasculature is not only highly variable, but even when all of the veins are identified, it can be difficult to transect each orthogonally in a reasonable amount of scan time. With interactive streamline rendering, it is possible to perform this analysis offline, carefully map where each pulmonary vein ultimately drains to, and quantify its individual contribution. We believe this may be helpful for both the pre-operative assessment and long-term follow-up of these patients after repair. It is also possible with this approach to determine the contribution of shunting of each of the shunt lesions that are simultaneously present. It is not uncommon, for example, for patients with PAPVR to present with multiple anomalous pulmonary veins and a concomitant sinus venosus ASD.[27,28]

In the evolution of our adoption of 4D-PC into our clinical-translational practice, we have seen a gradual transition in our perception and usage of this pulse sequence. We initially adopted 4D-PC as a purely research sequence. With experience, we transitioned to using it as an adjunct and problem-solving pulse sequence in situations where we had difficulty localizing occult shunts, or found disagreements between SSFP volumetry and 2D-PC flow measurements. With increasing confidence in the sequence and its postprocessing, we have further transitioned to using 4D-PC as the

workhorse of our congenital cardiac MRI examinations, placing it at the start of the exam, and in certain situations, as the sole diagnostic pulse sequence of the exam from which we obtain both flow measurements and ventricular volumetry.[12] To reach this end, we developed an in-line image reconstruction pathway to return an initial set of reconstructed images within 3–5 min of the image acquisition back to the scanner. This has allowed us to confirm adequate image quality and coverage to release patients following an abbreviated yet comprehensive exam in as short as 15 min. We suspect that there may be other clinical scenarios where a single 4D-PC acquisition may be sufficient to answer all the clinical questions that are posed in a request for a cardiac MRI. In many of our youngest patients with congenital heart disease, this approach has reduced overall imaging time, simplified image acquisition, and reduce the depth and duration of general anesthesia.

This work also presents our initial experience working with our variant of parallel-imaging compressed-sensing 4D-PC at 3T, supplementing our previous experience at 1.5T. Qualitatively, we have found that our approach yields higher signal-to-noise and velocity-to-noise results at higher field strengths, which we would expect with the SPGR-weighting of our imaging technique. It is possible though, that because smaller patients were triaged to our smaller-bore 3T scanner, some of the gains may have been due to differences in other aspects of the scanner configurations and patient body habitus. While we have not fully addressed the relationship between field strength and image quality in this particular

work, the images we have acquired thus far are promising for institutions seeking to perform cardiac imaging with 4D-PC at 3T. We further show in this work that venous flow measurements can be obtained with high internal consistency with combined parallel-imaging compressed-sensing, modest acceleration factors at arterial encoding speeds, but it is not clear that comparable flow measurements can be obtained with other implementations and more aggressive acceleration factors. Future work may be needed to fully assess differences in image quality, relative accuracy of flow quantification, and potential trade-offs at different field strengths.

Our study has some limitations. First, the sample population is fairly small. By design, as a retrospective study of our patients with known anomalous pulmonary veins, it includes a larger proportion of patients with shunt lesions than would be seen with a prospective study of suspected shunts. Because of this design, we are unable to directly assess the sensitivity or specificity of 4D-PC for detection of shunts in such a population. Future work will be required to separately assess these diagnostic parameters. In addition, we have not performed a comprehensive analysis of image quality and the patient and technical factors that can impact this. The technique used at our institution reflects a desire to simultaneously visualize the anatomic structures and obtain the 4D-PC vector field data in a single acquisition. Specifically, we have given blood pool contrast for our examinations and applied compressed-sensing and lower acceleration factors than reported at some other institutions.[10] Future studies may be required to determine whether these technical features are necessary for accurate flow quantification. It is possible that anatomic visualization may not be required for accurate flow measurement, particularly in larger vessels. Future work may be directed at determining the limits of quantitative accuracy using different 4D-PC approaches.

In conclusion, our study shows that venous shunt flow may be directly quantified with 4D-PC MRI. This helps to further validate the quantitative reliability of our approach and provides a roadmap for validation of other of implementations of 4D-PC for routine clinical use.

References

1. Festa P, Ait-Ali L, Cerillo AG, De Marchi D, Murzi B. Magnetic resonance imaging is the diagnostic tool of choice in the preoperative evaluation of patients with partial anomalous pulmonary venous return. Int J Cardiovasc Imaging 2006;22:685–693.

2. Riesenkampff EM-C, Schmitt B, Schnackenburg B, et al. Partial anomalous pulmonary venous drainage in young pediatric patients: the role of magnetic resonance imaging. Pediatr Cardiol 2009;30:458–464.

3. Robinson BL, Kwong RY, Varma PK, Wolfe M, Couper G. Magnetic resonance imaging of complex partial anomalous pulmonary venous return in adults. Circulation 2014;129:e1–e2.

4. Vyas H V, Greenberg SB, Krishnamurthy R. MR imaging and CT evaluation of congenital pulmonary vein abnormalities in neonates and infants. Radiographics 2012;32:87–98.

5. Fisher MR, Hricak H, Higgins CB. Magnetic resonance imaging of developmental venous anomalies. AJR Am J Roentgenol 1985;145:705–709.

6. Sigfridsson A, Petersson S, Carlhäll C-J, Ebbers T. Four-dimensional flow MRI using spiral acquisition. Magn Reson Med 2012;68:1065–1073.

7. Baltes C, Kozerke S, Hansen MS, Pruessmann KP, Tsao J, Boesiger P. Accelerating cine phase-contrast flow measurements using k-t BLAST and k-t SENSE. Magn Reson Med 2005;54:1430–1438.

8. Lustig M, Donoho D, Pauly JM. Sparse MRI: the application of compressed sensing for rapid MR imaging. Magn Reson Med 2007;58:1182–1195.

9. Dyvorne H, Knight-Greenfield A, Jajamovich G, et al. Abdominal 4D flow MR imaging in a breath hold: combination of spiral sampling and dynamic compressed sensing for highly accelerated acquisition. Radiology 2014;275:140973.

10. Vasanawala SS, Hanneman K, Alley MT, Hsiao A. Congenital heart disease assessment with 4D flow MRI. J Magn Reson Imaging 2015. [Epub ahead of print].

11. Hsiao A, Alley MT, Massaband P, Herfkens RJ, Chan FP, Vasanawala SS. Improved cardiovascular flow quantification with time-resolved volumetric phase-contrast MRI. Pediatr Radiol 2011;41:711–720.

12. Hsiao A, Lustig M, Alley MT, et al. Rapid pediatric cardiac assessment of flow and ventricular volume with compressed sensing parallel imaging volumetric cine phase-contrast MRI. AJR Am J Roentgenol 2012;198:W250–W259.

13. Hsiao A, Lustig M, Alley MT, Murphy MJ, Vasanawala SS. Evaluation of valvular insufficiency and shunts with parallel-imaging compressed-sensing 4D phase-contrast MR imaging with stereoscopic 3D velocity-fusion volume-rendered visualization. Radiology 2012;265:87–95.

14. Tariq U, Hsiao A, Alley M, Zhang T, Lustig M, Vasanawala SS. Venous and arterial flow quantification are equally accurate and precise with parallel imaging compressed sensing 4D phase contrast MRI. J Magn Reson Imaging 2012;37:1419–1426.

15. Valverde I, Simpson J, Schaeffter T, Beerbaum P. 4D phase-contrast flow cardiovascular magnetic resonance: comprehensive quantification and visualization of flow dynamics in atrial septal defect and partial anomalous pulmonary venous return. Pediatr Cardiol 2010;31:1244–1248.

16. Pelc NJ, Bernstein MA, Shimakawa A, Glover GH. Encoding strategies for three-direction phase-contrast MR imaging of flow. J Magn Reson Imaging 1991;1:405–413.

17. Vasanawala SS, Murphy MJ, Alley MT, et al. Practical parallel imaging compressed sensing MRI: summary of two years of experience in accelerating body MRI of pediatric patients. Proc IEEE Int Symp Biol Imaging 2011;2011:1039–1043.

18. Vasanawala SS, Alley MT, Hargreaves BA, Barth RA, Pauly JM, Lustig M. Improved pediatric MR imaging with compressed sensing. Radiology 2010;256:607–616.

19. Lustig M, Pauly JM. SPIRiT: iterative self-consistent parallel imaging reconstruction from arbitrary k-space. Magn Reson Med 2010;64:457–471.

20. Murphy M, Alley MT, Demmel J, Keutzer K, Vasanawala SS, Lustig M. Fast L1-SPIRiT compressed sensing parallel imaging MRI: scalable parallel implementation and clinically feasible runtime. IEEE Trasn Med Imaging 2012;31:1250–1262.

21. Bernstein MA, Zhou XJ, Polzin JA, et al. Concomitant gradient terms in phase contrast MR: analysis and correction. Magn Reson Med 1998;39:300–308.

22. Markl M, Bammer R, Alley MT, et al. Generalized reconstruction of phase contrast MRI: analysis and correction of the effect of gradient field distortions. Magn Reson Med 2003;50:791–801.

23. Walker PG, Cranney GB, Scheidegger MB, Waseleski G, Pohost GM, Yoganathan AP: semiautomated method for noise reduction and background phase error correction in MR phase velocity data. J Magn Reson Imaging 1993;3:521–530.

24. Hsiao A, Tariq U, Alley MT, Lustig M, Vasanawala SS. Inlet and outlet valve flow and regurgitant volume may be directly and reliably quantified with accelerated, volumetric phase-contrast MRI. J Magn Reson Imaging 2015;41:376–385.

25. Korkmaz AA, Yildiz CE, Onan B, Guden M, Cetin G, Babaoglu K. Scimitar syndrome: a complex form of anomalous pulmonary venous return. J Card Surg 2011;26:529–534.

26. Markl M, Frydrychowicz A, Kozerke S, Hope M, Wieben O. 4D flow MRI. J Magn Reson Imaging 2012;36:1015–1036.

27. Gustafson RA, Warden HE, Murray GF, Hill RC, Rozar GE. Partial anomalous pulmonary venous connection to the right side of the heart. J Thorac Cardiovasc Surg 1989;98(Pt 2):861–868.

28. Ho M-L, Bhalla S, Bierhals A, Gutierrez F. MDCT of partial anomalous pulmonary venous return (PAPVR) in adults. J Thorac Imaging 2009; 24:89–95.